Steel and Composite Structures, *Vol. 20, No. 6 (2016) 1237-1257*
DOI: http://dx.doi.org/10.12989/scs.2016.20.6.1237

Analysis of concrete shrinkage along truss bridge with steel-concrete composite deck

Wojciech Siekierski*

Institute of Civil Engineering, Poznań University of Technology, ul. Piotrowo 5, 61-138 Poznań, Poland

(*Received July 29, 2015, Revised February 09, 2016, Accepted February 15, 2016*)

Abstract. The paper concerns analysis of effects of shrinkage of slab concrete in a steel-concrete composite deck of a through truss bridge span. Attention is paid to the shrinkage alongside the span, i.e., transverse to steel-concrete composite cross-beams. So far this aspect has not been given much attention in spite of the fact that it affects not only steel-concrete decks of bridges but also steel-concrete floors of steel frame building structures. For the problem analysis a two-dimensional model is created. An analytical method is presented in detail. A set of linear equations is built to compute axial forces in members of truss girder flange and transverse shear forces in steel-concrete composite beams. Finally a case study is shown: test loading of twin railway truss bridge spans is described, verified FEM model of the spans is presented and computational results of FEM and the analytical method are compared. Conclusions concerning applicability of the presented analytical method to practical design are drawn. The presented analytical method provides satisfactory accuracy of results in comparison with the verified FEM model.

Keywords: concrete shrinkage; transverse shear forces; through truss bridge; steel-concrete composite deck

1. Introduction

European standards require railway bridges to have tracks placed in a gravel bed. To reduce construction depth the deck is often situated between a pair of main girders, near their bottom edges. In such cases concrete gravel bed of steel bridges is usually connected to cross-beams – steel-concrete composite deck. An example of such structure is a railway through truss bridge shown in Fig. 1.

The deck is connected to truss girder bottom flanges at their modes and between them. Since the flanges carry substantial bending their height is significantly larger than in classic truss girders. To limit dimensions of gusset plates the flanges are situated eccentrically in reference to the theoretical layout of truss members – Fig. 1, bottom left.

Usually joint action of the deck and truss girders occurs in the span type shown in Fig. 1. It is possible because shear connectors located at the interface of steel cross-beam and concrete slab transfer not only longitudinal shear forces (labelled "1" in Fig. 2(a)) but also transverse shear forces (labelled "2" in Fig. 2(a)). The longitudinal forces ("1") are caused mainly by cross-beam bending in vertical plane. The transverse shear forces ("2") occur due to span bending, uneven heating/cooling of the deck and girders as well as shrinkage of deck slab concrete.

*Corresponding author, Ph.D., E-mail: wojciech.siekierski@put.poznan.pl

 ISSN: 1229-9367 (Print), 1598-6233 (Online)

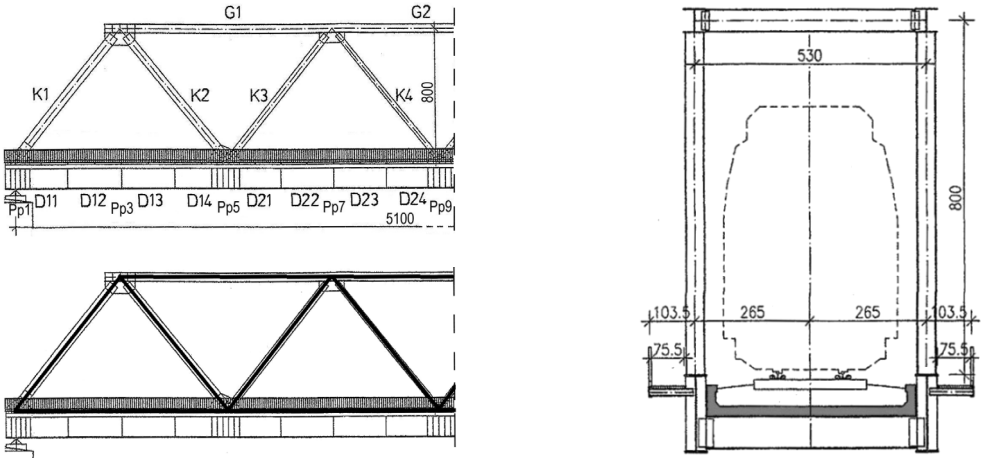

Fig. 1 An example of through truss railway bridge with steel-concrete composite deck: elevation (top left), cross-section (right) and theoretical layout of truss girder members (bottom left)

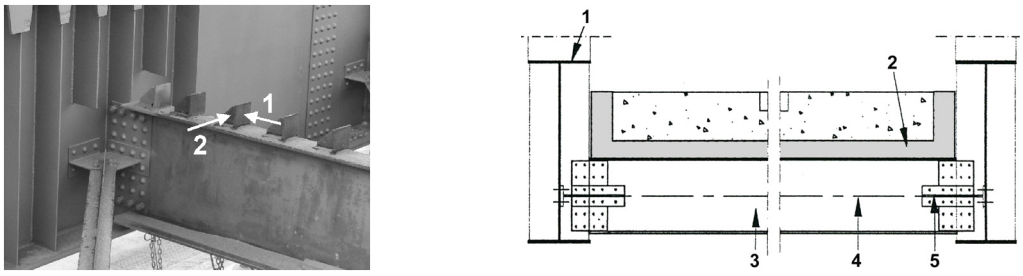

(a) (b)

Fig. 2 (a) Cross-beam to girder flange connection (symbols explained in the text); (b) Steel-concrete composite deck of a railway through truss bridge: 1 – bottom flange of a truss girder, 2 – RC deck slab, 3 – steel cross-beam, 4 –bottom wind bracing plane, 5 – wind bracing gusset plate

Intensity of the joint action of the deck and truss girders depends on the stiffness of connection between the deck and truss girder flanges adjacent to the deck. The stiffness depends on the torsional and flexural (in the horizontal plane) deformability of steel cross-beams within the width of the deck slab as well as the deformability of "connecting members". Such "connecting member" is shown in Figs. 2(a) and (b). It consists of a part of steel cross-beam beyond the outermost shear connector and the stiffening rib of truss girder flange. The cross-beam web is connected to the rib with a pair of steel plates. The connection is usually stiffened in horizontal plane by gusset plates of wind bracing – Fig. 2(b). Such arrangement of the connection is responsible for the cross-beam torsion – shear forces labelled "2" in Fig. 2(a) are applied to a cross-beam at the plane of its top flange while resultant shear forces at the cross-beam tips are transferred to truss girder flanges approximately at the half-height of the cross-beam web.

The joint action of the deck and truss girders provided by the „connecting members" unfavourably affects durability of the steel-concrete composite deck and its connection to truss girders. The unfavourable effects increase with span length. That is why bridge spans over 50 m long have the deck divided into sections with expansion joints in concrete slab – Fig. 3.

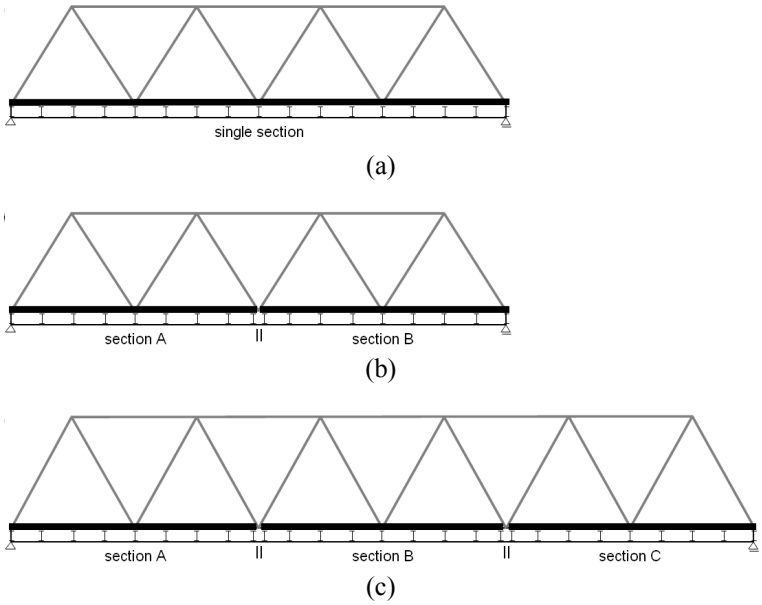

Fig. 3 Division of deck slab (darkened) into sections (symbols || mark expansion joints in concrete slab): (a) no expansion joints; (b) one expansion joint; (c) two expansion joints

2. Effects of shrinkage of concrete deck slab

Shrinkage of concrete slab of steel-concrete composite deck induces both types of shear forces at the steel-concrete interface (marked "1" and "2" in Fig. 2(a)). The effects of shrinkage alongside steel-concrete composite beams (in the direction of forces marked "1") have been investigated by Roll (1971), Montgomery *et al*. (1983) and Zuk (1961). Current analytical methods of analysis that account for material nonlinearities, time dependency and connectors flexibility have been applied by Johnson (1987), Bradford and Gilbert (1989), Gilbert and Bradford (1995), Ranzi and Bradford (2006). Recent analyses of concrete shrinkage effects in steel-concrete composite beams concern long-term flexural stiffness and have been presented by Fan *et al*. (2010a, b), Al-Deen *et al*. (2011a, b). Reviews of current achievements have been completed by Tanebe *et al*. (2009) and Ranzi *et al*. (2013). On the contrary the effects of concrete shrinkage in the direction transverse to a group of steel-concrete composite beams have not been investigated so far. The effects occur not only in such decks of bridge spans but also in steel structure buildings with steel-concrete composite floors.

The slab concrete shrinkage alongside a bridge span with steel-concrete composite deck (i.e., transverse to the cross-beams) causes the following:

- tension of concrete slab,
- bending of cross-beams in horizontal plane,
- torsion of cross-beams,
- compression and bending of main girders.

A method of analysis of the mentioned phenomena is described in the following chapters of this paper.

3. Assessment of concrete shrinkage effects with finite element method

Finite element method analyses of shrinkage effects in composite beams accounting for material nonlinearities, such as concrete cracking, connector flexibility have been reported by Kwak and Seo (2002), Fragiacomo *et al*. (2004), Virtuoso and Vieira (2004), Jurkiewiez *et al*. (2005), Ranzi (2006), Gara *et al*. (2006), Chaudhary *et al*. (2009), Sakr and Sakla (2008). However advanced and thorough the analyses are, their application in structural design and assessment of shrinkage effects in engineering structures is rather limited.

A useful method of FEM assessment of the effects of concrete shrinkage is based on application of an equivalent loading, as reported by Kianoush *et al*. (2008), Ma and Gao (2006). Namely it is uniform cooling applied to FE elements modelling concrete members. Since the coefficient of thermal expansion of concrete equals $\alpha = 1 \cdot 10^{-5} \frac{1}{^{\circ}C}$, the value of concrete shrinkage of $\varepsilon_s = 1 \cdot 10^{-5}$ refers to equivalent cooling of $T = 1°C$.

Such approach may be applied in the case of a concrete slab of steel-concrete composite decks in through truss bridges. To do so the concrete slab should be modelled with shell elements or brick elements.

4. Analytical method of assessment of concrete shrinkage effects

4.1 Initial assumptions

The described construction of steel-concrete composite deck and the way it is connected to truss girders require rather complex analysis, hardly useful in engineering practice. Thus some simplifying assumptions are made:

- effects of concrete shrinkage alongside a bridge span do not depend on concrete shrinkage across the bridge,
- concrete strain due to shrinkage is constant across the slab width,
- shear connectors at the steel-concrete interface are rigid – absence of concrete slab slip over steel cross-beams,
- steel-concrete composite cross-beams behave as rigid bodies in horizontal plane – absence of bending in horizontal plane and torsion.

4.2 Strain and deformation analysis

4.2.1 Computational model

Two-dimensional computational model is created to analyze effects of concrete shrinkage alongside a bridge span – Fig. 4. It refers to a half of a single section of a deck slab (Fig. 3) – between expansion joints – up to longitudinal symmetry axis. The model consists of deck slab (labelled "2" in Fig. 2(b)), cross-beams (labelled "3" in Fig. 2(b)) and the truss girder flange adjacent to the deck (labelled "1" in Fig. 2(b)) – the bottom flange is assumed. The flange is simply supported at its ends. Appropriate kinematical constraints are introduced along span longitudinal symmetry axis. The only load carried by the modelled structure is concrete shrinkage.

Fig. 4 shows numbering of slab spans (span …) and cross-beams (Pp…) as well as introduces the following symbols: E_a, E_c – elastic module of steel and concrete, respectively, $A_{a,i}$, A_c – cross-

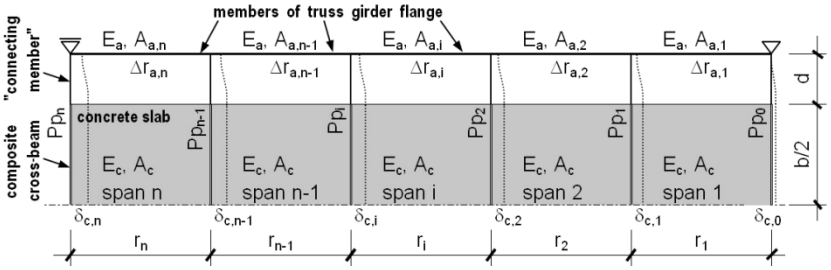

Fig. 4 Computational model for analysis of shrinkage of concrete slab in steel-concrete composite deck of a through truss bridge

section area of the *i*-th member of the truss girder flange adjacent to the deck and cross-section area of half of the deck slab respectively, r_i – lengths of the *i*-th deck slab span, equal to the length of the *i*-th member of the truss girder flange adjacent to the deck, $b/2$ – half of deck slab width, d – distance between truss girder longitudinal symmetry plane and the outermost shear connectors situated on steel-concrete composite cross-beams, $\delta_{c,i}$ – displacements of the *i*-th cross-beam, w_i – relative displacements alongside the bridge span of the tips of the *i*-th "connecting member", caused by its deformation in horizontal plane, $\Delta r_{a.i}$ – deformation of the *i*-th member of the truss girder flange adjacent to the deck.

The deformations $\delta_{c,i}$, w_i and $\Delta r_{a.i}$ result from the shrinkage of slab concrete alongside a bridge span.

4.2.2 Deformation of a "connecting member"

In general the ability of a planar computational model to replicate the response of the spatial system of through truss bridge span to concrete shrinkage is limited. In detail the flexural stiffness of a "connecting member" in horizontal plane and its torsional stiffness are difficult to establish precisely. The main reasons for that are plate action of flange rib, flexibility of steel-to-concrete connection in steel-concrete composite cross-beam and local stiffening provided by gusset plate of wind bracing. Hence the following technique is applied:

- the stiffness of a "connecting member" is taken as stiffness of steel cross-beam itself,
- variable boundary conditions for a "connecting member" are considered to take into account a spectrum of possible responses of through truss bridge span,
- three sets of boundary conditions in the horizontal plane for a "connecting member" are considered: fixed/fixed (Fig. 5(a)), fixed/hinged (Fig. 5(b)) and "averaged" of the two.

So the behaviour of a "connecting member" in the horizontal plane is described by the equation:

- for the fixed-fixed boundary conditions (Fig. 5(a))

Fig. 5 Boundary conditions for a "connecting member": (a) fixed/fixed; (b) fixed/hinged

$$w_i = P_i \cdot \frac{d^3}{12 \cdot E_a \cdot I_{ah}} \tag{1}$$

– for the fixed-hinged boundary conditions (Fig. 5(b))

$$w_i = P_i \cdot \frac{d^3}{3 \cdot E_a \cdot I_{ah}} \tag{2}$$

– for the "averaged" of the two above

$$w_i = \frac{1}{2} \cdot \left(P_i \cdot \frac{d^3}{12 \cdot E_a \cdot I_{ah}} + P_i \cdot \frac{d^3}{3 \cdot E_a \cdot I_{ah}} \right) = P_i \cdot \frac{5 \cdot d^3}{24 \cdot E_a \cdot I_{ah}} \tag{3}$$

where: w_i – deformation of the i-th "connecting member" (m), P_i – horizontal force acting perpendicular to the i-th cross-beam (kN), d – length of the "connecting member" (m), E_a – modulus of elasticity for steel (MPa), I_{ah} – moment of inertia of the "connecting member" in bending in horizontal plane (m^4).

The force P_i equals the difference of longitudinal forces in the members of truss girder adjacent to the cross-beam in question

$$P_i = P_{a,i} - P_{a,i+1} \tag{4}$$

For clarity of notation the following coefficient is introduced

$$\beta = \begin{cases} \dfrac{d^3}{12 \cdot E_a \cdot I_{ah}} & \text{for fixed/fixed boundary conditions} \\ \dfrac{d^3}{3 \cdot E_a \cdot I_{ah}} & \text{for fixed/hinged boundary conditions} \\ \dfrac{5 \cdot d^3}{24 \cdot E_a \cdot I_{ah}} & \text{for "averaged" boundary conditions} \end{cases} \tag{5}$$

So the displacement w_i equals

$$w_i = \left(P_{a,i} - P_{a,i+1} \right) \cdot \beta \tag{6}$$

4.2.3 Deformation of members of truss girder flange

The slab concrete shrinkage induces tension of the slab as well as compression and bending of truss girders. Fig. 6 shows effects of slab concrete shrinkage (marked with white arrows) in a through truss bridge with composited deck. The shrinkage generates internal forces in the concrete slab and truss girder members. Only dominant internal forces, i.e., axial forces, are analysed. The symbols in Fig. 6 are: P_c – axial force in concrete slab due to shrinkage, P_{a1}, P_a, P_d – axial forces in the top flange, the bottom flange and the diagonal bracing respectively, z_c – distance between neutral axes of truss girder and concrete slab centre plane, z_a – distance between neutral axes of truss girder and bottom flange centre line, h_t – truss girder theoretical height, h_c – distance between neutral axis of top flange and centre plane of concrete slab, h_a – distance between neutral axes of top and bottom flange.

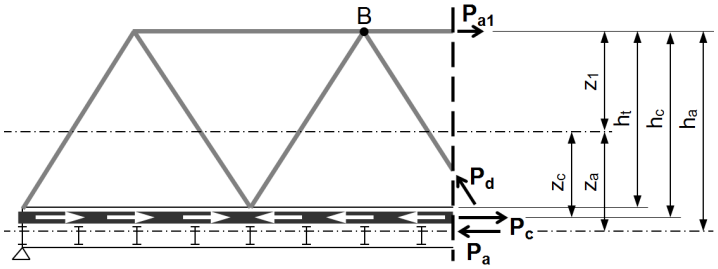

Fig. 6 Analysis of forces in truss girder members due to shrinkage of slab concrete

The equilibrium of moments of forces in respect to point B requires

$$P_c \cdot h_c - P_a \cdot h_a = 0, \tag{7}$$

so

$$P_c = P_a \cdot \frac{h_a}{h_c}. \tag{8}$$

The strain at the neutral axis of the *i*-th member of the truss girder bottom flange caused by shrinkage of slab concrete is given as

$$\varepsilon_{a,i} = \frac{\Delta r_{a.i}}{r_i} = \frac{P_{c,i}}{E_a \cdot A_a} + \frac{P_{c,i} \cdot z_c}{E_a \cdot I} \cdot z_a, \tag{9}$$

where: $\Delta r_{a,i}$ – deformation (shortening) of the *i*-th member of truss girder flange due to shrinkage of slab concrete (m), I – moment of inertia of the truss girder (m^4), A_a – average cross-sectional area of the truss girder flanges (m^2).

Substituting Eq. (8) for P_c in Eq. (9) gives

$$\varepsilon_{a,i} = \frac{\Delta r_{a.i}}{r_i} = \frac{P_{a,i} \cdot \frac{h_a}{h_c}}{E_a \cdot A_a} + \frac{P_{a,i} \cdot \frac{h_a}{h_c} \cdot z_c \cdot z_a}{E_a \cdot I}, \tag{10}$$

The value of z_a may be computed as

$$z_a = \frac{A_t \cdot h_a}{A_t + A_b}, \tag{11}$$

where: A_t, A_b – averaged cross-sectional area of top and bottom flange of truss girder respectively (m^2).

The moment of inertia of the truss girder equals

$$I = I_t + A_t \cdot \left(h_a - z_a\right)^2 + I_b + A_b \cdot {z_a}^2, \tag{12}$$

where: I_t, I_b – an average moments of inertia of top and bottom flanges of the truss girder respectively.

Diagonal members of trusses provide smaller shear stiffness in comparison to the web of a similar plate girder. Hence, effective moment of inertia of the truss girder is smaller than given by the Eq. (12). The difference depends on truss static scheme – type of supports and loading. In the case of bridge truss girders, a simply supported and uniformly loaded beam may be assumed as representative scheme. For such conditions the moment of inertia of a truss girder reflecting its actual shear stiffness, given by Pałkowski (2001), is

$$I_v = \frac{I}{1 + \frac{48}{5} \cdot \frac{E_a \cdot I}{S_v \cdot L_t^{\,2}}}, \tag{13}$$

where: I_v – moment of inertia of the truss girder reflecting its actual shear stiffness (m^4), L_t – theoretical span length of the truss girder (m), S_v – shear stiffness coefficient of the truss girder (kN).

For the truss girder with parallel flanges and "*W*" bracing the shear stiffness coefficient is given by Pałkowski (2001) as

$$S_v = E_a \cdot A_d \cdot \sin^2(\alpha) \cdot \cos(\alpha), \tag{14}$$

where: α – an inclination angle of diagonal bracing members (degrees), A_d – an average cross-sectional area of diagonal members (m^2).

Finally, the deformation of the *i*-th member of the truss girder flange is given as

$$\Delta r_{a.i} = P_{a,i} \cdot \left(\frac{\frac{h_a}{h_c} \cdot r_i}{E_a \cdot A_a} + \frac{\frac{h_a}{h_c} \cdot z_c \cdot z_a \cdot r_i}{E_a \cdot I_v} \right). \tag{15}$$

Since all slab spans are usually equal in length the auxiliary coefficient γ is introduced

$$\gamma = \frac{\frac{h_a}{h_c} \cdot r}{E_a \cdot A_a} + \frac{\frac{h_a}{h_c} \cdot z_c \cdot z_a \cdot r}{E_a \cdot I_v}, \tag{16}$$

where r is slab span length. Then

$$\Delta r_{a.i} = P_{a,i} \cdot \gamma. \tag{17}$$

4.2.4 Moment of inertia of the truss girder near support

The height of the girders with "*W*" bracing (Figs. 1 and 6) decreases linearly near supports from theoretical height at the end of a top flange to zero at supports, i.e., over the length of support diagonal.

The equivalent moment of inertia valid over the outermost slab span (I_{eq1}) is computed based on cantilever analogy. The trussed system and the cantilever of equivalent moment of inertia are shown Fig. 7.

In the trussed system shown in Fig. 7 (top) the force T generates:
– horizontal reactions R

$$R = T \cdot \frac{r}{h'_t}, \tag{18}$$

– compressive axial force in the outermost member of bottom flange

$$N_{b1} = R, \tag{19}$$

– tensile axial force in the support diagonal

$$N_{d1} = \frac{T}{\sin(\alpha)}, \tag{20}$$

– bending moment in the outermost member of bottom flange (constant along its length)

$$M_{b1} = R \cdot z_t. \tag{21}$$

The length of the support diagonal over the outermost slab span

$$l_{d1} = \frac{h'_t}{\sin(\alpha)}. \tag{22}$$

Vertical displacement under the force T is computed based on virtual work principle. Internal forces generated by the force T and virtual force $\bar{1}$ pointing downwards are put together in Table 1. Note: all axial forces and bending moments are constant over the given member length.

Based on the data given in Table 1 one may compute the displacement v

$$v = \frac{\frac{T}{\sin(\alpha)} \cdot \frac{h'_t}{\sin(\alpha)} \cdot \frac{\bar{1}}{\sin(\alpha)}}{E_a \cdot A_{d1}} + \frac{T \cdot r \cdot \bar{1} \cdot \left(\frac{r}{h'_t}\right)^2}{E_a \cdot A_{b1}} + \frac{T \cdot r \cdot \bar{1} \cdot \left(\frac{r}{h'_t} \cdot z_t\right)^2}{E_a \cdot I_{b1}}. \tag{23}$$

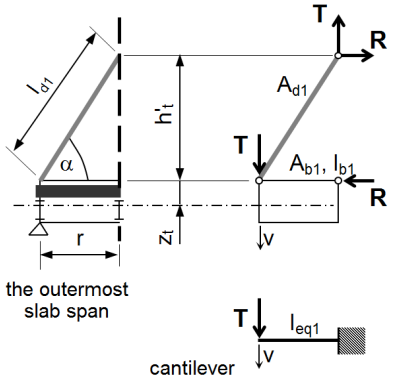

Fig. 7 Computational model for setting flexural stiffness of truss girder near support

Table 1 Data to compute the displacement v (Fig. 7)

Member	Member length	Stiffness	Axial force or bending moment (last row) generated by	
			T	$\bar{1}$
The support diagonal over the outermost slab span	$\frac{h'_t}{\sin(\alpha)}$	$E_a \cdot A_{k1}$	$\frac{T}{\sin(\alpha)}$	$\frac{\bar{1}}{\sin(\alpha)}$
The outermost member of bottom flange	r	$E_a \cdot A_{b1}$	$T \cdot \frac{r}{h'_t}$	$\bar{1} \cdot \frac{r}{h'_t}$
The outermost member of bottom flange	r	$E_a \cdot I_{b1}$	$T \cdot \frac{r}{h'_t} \cdot z_t$	$\bar{1} \cdot \frac{r}{h'_t} \cdot z_t$

Rearranging

$$v = \frac{T}{E_a} \cdot \left(\frac{\frac{h'_t}{\sin^3(\alpha)}}{A_{d1}} + \frac{\frac{r^3}{h'^2_t}}{A_{b1}} + \frac{\frac{r^3 \cdot z_t^2}{h'^2_t}}{I_{b1}} \right). \tag{24}$$

In the case of the cantilever shown in Fig. 7 (bottom) the displacement of its tip equals

$$v = \frac{T}{E_a} \cdot \frac{r^3}{3 \cdot I_{eq1}}. \tag{25}$$

Comparing right sides of the Eqs. (24) and (25) the equivalent moment of inertia I_{eq1} equals

$$I_{eq1} = \frac{r^3}{3 \cdot \left(\frac{h'_t}{A_{d1} \cdot \sin^3(\alpha)} + \frac{r^3}{A_{pd} \cdot h'^2_t} + \frac{r^3 \cdot z_t^2}{I_{pd} \cdot h'^2_t} \right)}. \tag{26}$$

If the support diagonal covers more than one slab span then the moments of inertia for the truss girder within consecutive spans may be computed as linear interpolation between I_{eq1} and I_v.

4.3 Internal forces caused by concrete shrinkage alongside a bridge span

In the computational model shown in Fig. 4 the shrinkage of slab concrete causes:

- tension of the deck slab,
- bending of the „connecting members" in horizontal plane,
- compression of members of the truss girder flange adjacent to the deck.

Carrying out the analysis presented in the Chapter 4.2.3 for truss girder members within each span of concrete slab leads to the set of equilibrium equations similar to the Eq. (8)

$$\begin{aligned}
&P_{c,1} - P_{a,1} \cdot \frac{h_a}{h_c} = 0 \\
&P_{c,2} - P_{a,2} \cdot \frac{h_a}{h_c} = 0 \\
&\vdots \\
&P_{c,i} - P_{a,i} \cdot \frac{h_a}{h_c} = 0 \\
&\vdots \\
&P_{c,n} - P_{a,n} \cdot \frac{h_a}{h_c} = 0
\end{aligned} \tag{27}$$

where: $P_{c,i}$ – tensile axial force in the i-th span of concrete slab (kN), $P_{a,i}$ – compressive axial force in the i-th member of the truss girder bottom flange (kN).

The axial forces may be expressed as functions of strains and displacements.

Axial forces in the concrete slab

The forces may be expressed based on Hooke's law, with total strain being resultant of the concrete shrinkage strain (ε_s) and composited cross-beam displacements ($\delta_{c,i}$) alongside a bridge span (Fig. 4)

$$\begin{aligned}
P_{c,1} &= \left(\varepsilon_s - \frac{\delta_{c,1}}{r_1} + \frac{\delta_{c,0}}{r_1} \right) \cdot E_c \cdot A_c \\
P_{c,2} &= \left(\varepsilon_s - \frac{\delta_{c,2}}{r_2} + \frac{\delta_{c,1}}{r_2} \right) \cdot E_c \cdot A_c \\
&\vdots \\
P_{c,i} &= \left(\varepsilon_s - \frac{\delta_{c,i}}{r_i} + \frac{\delta_{c,i-1}}{r_{i-1}} \right) \cdot E_c \cdot A_c \\
&\vdots \\
P_{c,n} &= \left(\varepsilon_s - \frac{\delta_{c,n}}{r_{n-1}} + \frac{\delta_{c,n-1}}{r_{n-1}} \right) \cdot E_c \cdot A_c
\end{aligned} \tag{28}$$

Usually all slab spans have the same length. Thus an auxiliary coefficient η may be introduced

$$\eta = \frac{E_c \cdot A_c}{r}. \tag{29}$$

So the Eq. (28) are

$$\begin{aligned}
P_{c,1} &= \left(r \cdot \varepsilon_s - \delta_{c,1} + \delta_{c,0} \right) \cdot \eta \\
P_{c,2} &= \left(r \cdot \varepsilon_s - \delta_{c,2} + \delta_{c,1} \right) \cdot \eta \\
&\vdots
\end{aligned} \tag{30}$$

$$\begin{aligned} P_{c,i} &= \left(r \cdot \varepsilon_s - \delta_{c,i} + \delta_{c,i-1}\right) \cdot \eta \\ &\vdots \\ P_{c,n} &= \left(r \cdot \varepsilon_s - \delta_{c,n} + \delta_{c,n-1}\right) \cdot \eta \end{aligned} \tag{30}$$

Axial forces in the members of the truss girder bottom flange

According to the Eq. (17) the forces may be expressed as

$$P_{a,i} = \frac{\Delta r_{a.i}}{\gamma}. \tag{31}$$

The changes of lengths of the truss girder members may be expressed as functions of displacements of steel-concrete composite cross-beams and deformations of the "connecting members"

$$\Delta r_{a.i} = \delta_{c.i} - \delta_{c.i-1} - (w_i - w_{i-1}), \tag{32}$$

where displacements w_i are given according to the Eq. (6).

Substituting Eq. (32) for $\Delta r_{a.i}$ in Eq. (31) one may write the equation for each member of the truss girder bottom flange

$$\begin{aligned} P_{a,1} &= \frac{\delta_{c,1} - \delta_{c,0} - \left(P_{c,1} - P_{c,2}\right) \cdot \beta + \left(0 - P_{c,1}\right) \cdot \beta}{\gamma} \\ P_{a,2} &= \frac{\delta_{c,2} - \delta_{c,1} - \left(P_{c,2} - P_{c,3}\right) \cdot \beta + \left(P_{c,1} - P_{c,2}\right) \cdot \beta}{\gamma} \\ &\vdots \\ P_{a,i} &= \frac{\delta_{c,i} - \delta_{c,i-1} - \left(P_{c,i} - P_{c,i+1}\right) \cdot \beta + \left(P_{c,i-1} - P_{c,1}\right) \cdot \beta}{\gamma} \\ &\vdots \\ P_{a,n} &= \frac{\delta_{c,n} - \delta_{c,n-1} - \left(P_{c,n} - 0\right) \cdot \beta + \left(P_{c,n-1} - P_{c,n}\right) \cdot \beta}{\gamma} \end{aligned} \tag{33}$$

After rearranging the equations are

$$\begin{aligned} P_{a,1} &= \frac{\delta_{c,1} - \delta_{c,0} - \left(2 \cdot P_{c,1} - P_{c,2}\right) \cdot \beta}{\gamma} \\ P_{a,2} &= \frac{\delta_{c,2} - \delta_{c,1} - \left(2 \cdot P_{c,2} - P_{c,1} - P_{c,3}\right) \cdot \beta}{\gamma} \\ &\vdots \\ P_{a,i} &= \frac{\delta_{c,i} - \delta_{c,i-1} - \left(2 \cdot P_{c,i} - P_{c,i-1} - P_{c,i+1}\right) \cdot \beta}{\gamma} \\ &\vdots \\ P_{a,n} &= \frac{\delta_{c,n} - \delta_{c,n-1} - \left(2 \cdot P_{c,n} - P_{c,n-1}\right) \cdot \beta}{\gamma} \end{aligned} \tag{34}$$

Substituting Eq. (30) for $P_{c,i}$ in Eq. (34) gives axial forces in the members of the truss girder bottom flange ($P_{a,i}$) as functions of the displacements of the composited cross-beams ($\delta_{c,i}$) and the concrete shrinkage strain (ε_s)

$$\begin{aligned}
P_{a,1} &= \frac{\delta_{c,1} - \delta_{c,0} - \left(r \cdot \varepsilon_s + 2 \cdot \delta_{c,0} - 3 \cdot \delta_{c,1} + \delta_{c,2}\right) \cdot \eta \cdot \beta}{\gamma} \\
P_{a,2} &= \frac{\delta_{c,2} - \delta_{c,1} - \left(-\delta_{c,0} + 3 \cdot \delta_{c,1} - 3 \cdot \delta_{c,2} + \delta_{c,3}\right) \cdot \eta \cdot \beta}{\gamma} \\
&\vdots \\
P_{a,i} &= \frac{\delta_{c,i} - \delta_{c,i-1} - \left(-\delta_{c,i-2} + 3 \cdot \delta_{c,i-1} - 3 \cdot \delta_{c,i} + \delta_{i+1}\right) \cdot \eta \cdot \beta}{\gamma} \\
&\vdots \\
P_{a,n} &= \frac{\delta_{c,n} - \delta_{c,n-1} - \left(r \cdot \varepsilon_s - \delta_{c,n-2} + 3 \cdot \delta_{c,n-1} - 2 \cdot \delta_{c,n}\right) \cdot \eta \cdot \beta}{\gamma}
\end{aligned} \tag{35}$$

Displacements of the outermost cross-beam Pp_0

Due to assumed kinematical constrains the displacement $\delta_{c,0}$ equals the deformation of the "connecting member" under force $P_{c,1}$

$$\delta_{c,0} = -P_{c,1} \cdot \beta, \tag{36}$$

where: $P_{c,1}$ – axial force in the span 1 of the concrete slab (see Fig. 4).

4.4 Effects of concrete shrinkage alongside a bridge span

Eqs. (27) and (36) form a set of linear equations

$$\begin{cases}
P_{c,1} - P_{a,1} \cdot \dfrac{h_a}{h_c} = 0 \\
P_{c,2} - P_{a,2} \cdot \dfrac{h_a}{h_c} = 0 \\
\vdots \\
P_{c,i} - P_{a,i} \cdot \dfrac{h_a}{h_c} = 0 \\
\vdots \\
P_{c,n} - P_{a,n} \cdot \dfrac{h_a}{h_c} = 0 \\
P_{c,1} \cdot \beta = -\delta_{c,0}
\end{cases} \tag{37}$$

Substituting Eqs. (30) and (35) for $P_{c,i}$ and $P_{a,i}$ respectively in the set Eq. (37) gives a set of n+1 equations with n+1 unknowns $\delta_{c,i}$. There is a unique solution.

To find axial forces in the concrete slab spans ($P_{c,i}$) and in the members of truss girder bottom flange ($P_{a,i}$) one may use Eqs. (30) and (35). Axial forces in slab spans enable computation of transverse shear forces in composited cross-beams

$$\begin{aligned} V_0 &= -P_{c,1} \\ V_1 &= P_{c,1} - P_{c,2} \\ &\vdots \\ V_i &= P_{c,i} - P_{c,i+1} \\ &\vdots \\ V_{n-1} &= P_{c,n-1} - P_{c,n} \\ V_n &= P_n \end{aligned} \tag{38}$$

where: V_i – total transverse shear force in the i-th composited cross-beam (kN); it is a load acting on shear connectors over half of i-th cross-beam length in the transverse direction.

5. Case study – verification of the analytical method

5.1 Introduction

The presented analytical method was verified indirectly with the results of test loading of twin railway truss bridge spans with steel-concrete composite decks. The indirect verification means that:

- test loading of the twin spans was carried out,
- results of the test loading were used to verify a FEM model of the bridge spans,
- the verified FEM model was then used for verification of the presented analytical method.

5.2 Analyzed bridge spans

Test loading of the twin railway truss bridge spans with composited deck was carried out. The structure of the spans is shown in Fig. 1. Dimensions and details are as follows:

- theoretical length: 51.0 m,
- truss theoretical height: 8.00 m,
- distance between centres of gravity of top and bottom flange: 8,85 m,
- truss girder spacing: 5.30 m,
- flange node spacing: 12.75 m,
- cross-beam spacing: 3.19 m,
- deck slab: 25÷33 cm thick, made of C30/35 class concrete, reinforced with 64 ϕ25 steel bars in two layers (near top and bottom of the slab), divided into two sections – transverse expansion joint in the middle of the span – as in Fig. 3(b).

Cross-sectional characteristics of structural members are given in Table 2. Indices: (1) half of the member length near D11; (2) half of the member length near D13; (3) half of the member

Table 2 Cross-sectional characteristics of main structural members

Member (see Fig. 1a for symbols)	A_X [cm^2]	I_X [cm^4]	I_Y [cm^4]	I_Z [cm^4]
D11, D12[1)]	364	231	1669197	33358
D12[2)], D13, D14[3)]	394	337	1878496	39608
D14[4)], D21[5)]	494	1012	2586517	60441
D21[6)], D22÷D24	474	794	2466298	56274
G1	310	432	158183	41711
G2	405	958	221373	58398
K1	244	243	87208	37514
K2	184	110	59471	25014
K3	134	58	40572	12803
K4	98	32	27393	4503
Pp (steel cross beam)	170	150	157119	5439
Deck slab	description in the text			

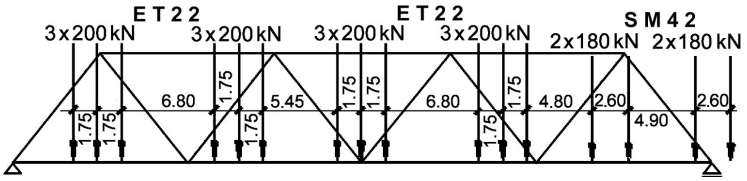

Fig. 8 Test loading layout

length near D13; (4) half of the member length near D21; (5) half of the member length near D14; (6) half of the member length near D22. Note: the axis OY is horizontal and perpendicular to webs of members D, G, K and Pp.

The same locomotive set, shown in Fig. 8, was used for both spans. In the case of both spans, railway track is located symmetrically between truss girders. It may be concluded that four truss girders were test loaded in the same way.

During testing the following were recorded:

- vertical displacement of bottom flange nodes, at: ¼·L_t, ½·L_t, ¾·L_t (where L_t is the theoretical span length) under loading as in Fig. 8,
- strains at the top fibres of truss bottom flanges at the cross-section located 3.5 m away from the D14/D21 node (Fig. 1) towards midspan, during locomotive set crossing the span at very low speed (≤ 5 km/h) – quasi-static loading.

5.3 Computational model of finite element method

The FEM computational model of test loaded bridge spans was created in *Autodesk Robot* package (2013). It is shown in Fig. 9.

Members of truss girders, cross-beams, wind bracings were modelled with 2-node beam elements of general purpose. Their characteristics were taken as in Table 2 (the symbols according

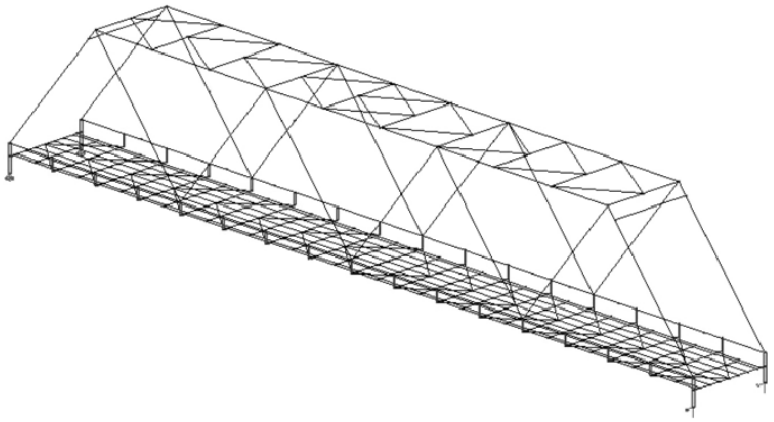

Fig. 9 Computational model of finite element method

to Fig. 1). The deck slab was modelled with 4-node thin shell elements – 8 elements across and 32 elements along the slab. Slab width was assumed as 4.7 m, and thickness – variable, from 29.5 cm for the elements near the width centre up to 31.0 cm for the elements near slab side edges.

The computational model reflects eccentricities of bottom flange at their connections to diagonal members as well as actual levels of neutral axes of bottom flange members, cross-beams, bottom wind bracing and actual level of bearings. Tip nodes of the outermost elements modelling cross-beams and respective nodes of elements modelling bottom flange are mutually constrained to assure compatibility of deformations. In Fig. 9 the kinematical constraints are marked with short vertical lines connecting bottom flange nodes and cross-beam tips.

In the model it is assumed that the characteristics of the "connection members" are the same as respective characteristics of steel cross-beams.

Results recorded during test loading and computed are put together in Tables 3 and 4. Table 3 gives vertical displacements of bottom flange nodes and Table 4 – extreme values of normal stress

Table 3 Vertical displacements u [mm] of bottom flange nodes

Result	Location of bottom flange nodes		
	$¼ \cdot L_t$	$½ \cdot L_t$	$¾ \cdot L_t$
u_{comp}	9,37	13,24	9,23
u_{rec}	8,16	11,78	8,07
u_{comp} / u_{rec}	1,15	1,12	1,14

Table 4 Extreme values of normal stress in the top fibre of bottom flange

Result	Extreme values of normal stress σ [MPa] (see Fig. 10)				
	I	II	III	IV	V
σ_{comp}	6,8	11,5	8,7	9,9	9,0
σ_{rec}	4,4	10,5	8,9	10,1	8,4
$\sigma_{comp} / \sigma_{rec}$	1,55	1,10	0,98	0,98	1,07

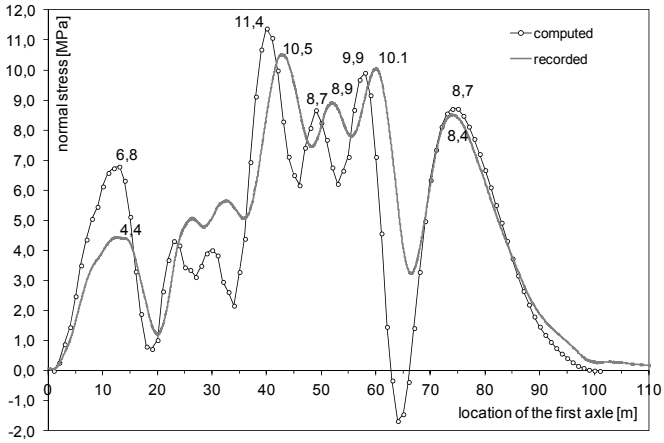

Fig. 10 Stress variation in top fibre of bottom flange at the instrumented cross-section during passage of test loading along the span

at the top fibre of bottom flange at the instrumented cross-section (stress variation diagram is given in Fig. 10). Both tables give also the relationship of computed and recorded values. Tables 3 and 4 show that computational results provided by the FEM model comply with recorded data well.

The presented FEM model was then used for computation of effects of shrinkage of concrete slab alongside the bridge span. The shrinkage of 0,0002 was represented in the model by slab cooling of $\Delta T = -20°C$.

5.4 Computational model of the analytical method

The deck slab is divided into two identical sections. The analysis concerns one of them. The

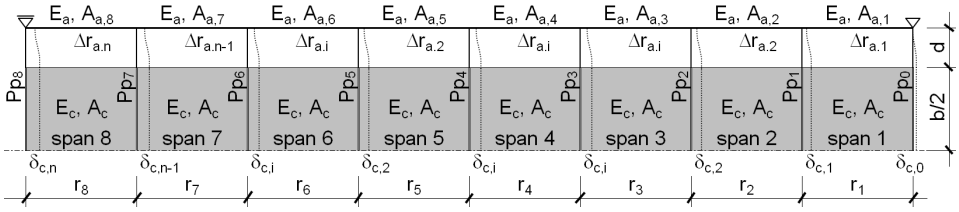

Fig. 11 Computational model of analytical method

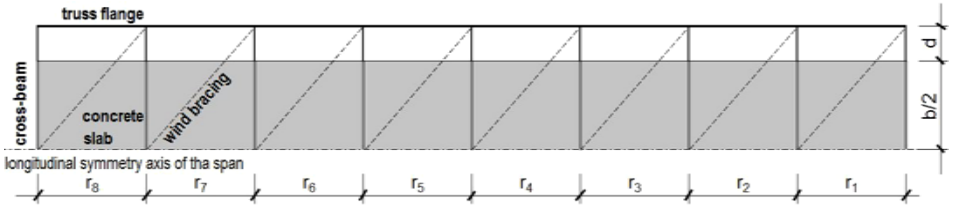

Fig. 12 Arrangement of structural members of analysed steel-concrete composite deck

computational model is shown in Fig. 11 and structural member arrangement – in Fig. 12. It can be seen that besides previously stated assumptions wind bracing are neglected in the computational model.

Characteristics of elements shown in Fig. 11 are as in Table 2. The actual width of concrete slab is taken into account while its thickness is averaged – 30 cm.

Cross-sectional areas and moments of inertia of flanges and diagonal members for computing the moment of inertia of the truss girder (over its part where flanges are parallel) are taken as weighted average of respective characteristics. Variation of moment of inertia of truss girder within support diagonal length is reflected.

Deformations of the "connecting members" are defined for two alternative patterns of boundary conditions. Within each of them the behaviour of outermost "connecting members" differ from the behaviour of intermediate ones. This reflects the fact that the outermost "connecting members" arte situated near concrete slab edges. In the pattern A the outermost "connecting members" are assumed to behave as the beam in Fig. 5(b) while behaviour of the others is assumed as "averaged". In the pattern B the behaviour of the outermost "connecting members" is assumed as "averaged" while the others are assume to behave as the beam in Fig. 5(a).

5.5 Comparison of computed results

The results obtained from both models are compared in diagrams. The diagrams show:

– values of compressive axial forces in the members of bottom flange (Fig. 13),
– values of total shear forces transverse to composited cross-beams (Fig. 14).

Results of pattern A and B of boundary conditions of the "connecting members" in the analytical method are distinguished.

Fig. 13 shows that pattern B of analytical method and the FEM model give similar assessment of axial forces in bottom flange in terms of quality of results. Discrepancies fall within the range from –15% (underestimation) up to +8% (overestimation) in respect to the FEM results. In the case of pattern A of analytical method the discrepancies are significantly bigger (the analytical method underestimates results).

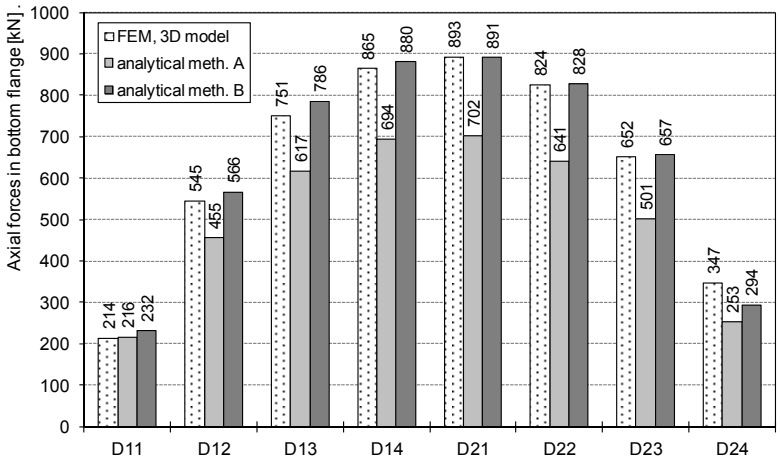

Fig. 13 Axial forces in members of bottom flange

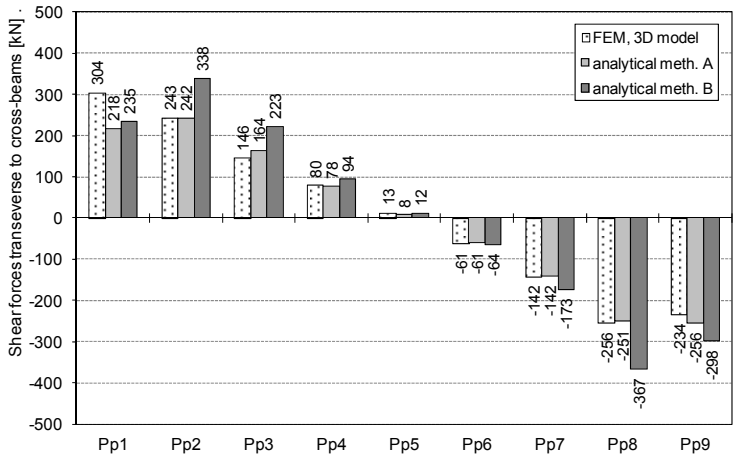

Fig. 14 Total shear forces transverse to composited cross-beams (positive sign means that given force points right)

Fig. 14 shows that pattern A of analytical method and the FEM model give similar distribution of transverse shear forces. Discrepancies fall within the range from -28% up to +9% in respect to the FEM results. In the case of pattern B of analytical method the discrepancies are bigger locally – particularly for slab spans adjacent to the outermost ones. In spite of that, for practical purposes, the results of pattern B are applicable for design. Since all cross-beams are usually identical the most unfavourable shear force obtained governs the design. For the pattern B the overestimation is about 20% while pattern A gives underestimation of about 16% with respect to FEM model results.

The reasons for the reported discrepancies are:

(a) deformability of deck slab across its width in its plane,
(b) torsion and constrained bending of cross-beams in horizontal plane due to wind bracing,
(c) spatial, instead of planar, response of the steel structure do deck slab shrinkage.

6. Conclusions

Analysis of effects of concrete shrinkage alongside a through truss bridge span with steel-concrete composite deck is possible with an aid of 2D analytical model. The model consists of half of width of the deck and adjacent truss girder flange.

Concrete shrinkage acts on the 3D system of though truss bridge span. This makes difficult to replicate its response with 2D computational model. To cope with the problem variant analysis is applied – two computational models with different patterns of boundary conditions of the "connecting members" in horizontal plane are considered. For the analysed bridge spans the pattern B turned out to be applicable to practical design.

It is possible to improve the 2D model of analytical method by taking into account torsional and flexural (in the horizontal plane) deformability of steel cross-beams. In general it will reduce the intensity of the joint action of the steel-concrete composite deck and the truss girders. Internal forces in the deck slab and the adjacent members of truss girder flanges due to concrete shrinkage will decrease while their distribution may change moderately.

The presented analytical method is applicable also to plate girder spans with steel-concrete composite decks as well as steel-concrete composite floors of steel frame building structures.

Acknowledgments

The support of the 503213/01/12/DS-PB/0409/14 grant of the Ministry of Science and Higher Education of Republic of Poland is kindly acknowledged.

References

Autodesk Robot (2013), http://usa.autodesk.com/adsk/servlet/index?siteID=123112&id=13093279

Al-Deen, S., Ranzi, G. and Vrcelj, Z. (2011a), "Full-scale long-term experiments of simply supported composite beams with solid slabs", *J. Construct. Steel Res.*, **67**(3), 308-321.

Al-Deen, S., Ranzi, G. and Vrcelj, Z. (2011b), "Shrinkage effects on flexural stiffness of composite beams with solid concrete slabs: An experimental study", *Eng. Struct.*, **33**(4), 1302-1315.

Bradford, M.A. and Gilbert, R.I. (1989), "Non-linear behaviour of composite beams at service loads", *Struct. Eng.*, **67**(14), 263-268.

Chaudhary, S., Pendharkar, U. and Nagpal, A.K. (2009), "Control of creep and shrinkage effects in steel concrete composite bridges with precast decks", *J. Bridge Eng.*, *ASCE*, **14**(5), 336-345.

Fan, J., Nie, X., Li, Q. and Li, Q. (2010a), "Long-term behavior of composite beams under positive and negative bending. I: experimental study", *J. Struct. Eng.*, *ASCE*, **136**(7), 849-857.

Fan, J., Nie, X., Li, Q. and Li, Q. (2010b), "Long-term behavior of composite beams under positive and negative bending. II: Analytical study", *J. Struct. Eng.*, *ASCE*, **136**(7), 858-865.

Fragiacomo, M., Amadio, C. and Macorini, L. (2004), "Finite-element model for collapse and long-term analysis of steel–concrete composite beams", *J. Struct. Eng.*, *ASCE*, **130**(3), 489-497.

Gara, F., Ranzi, G. and Leoni, G. (2006), "Time analysis of composite beams with partial interaction using available modelling techniques: A comparative study", *J. Construct. Steel Res.*, **62**(9), 917-930.

Gilbert, R.I. and Bradford, M.A. (1995), "Time-dependent behaviour of continuous composite beams at service loads", *J. Struct. Eng. ASCE*, **121**(2), 319-327.

Johnson, R.P. (1987), "Shrinkage-induced curvature in composite beams with a cracked concrete flange", *Struct. Eng.*, **65**(4), 72-77.

Jurkiewiez, B., Buzon, S. and Sieffert, J.G. (2005), "Incremental viscoelastic analysis of composite beams with partial interaction", *Comput. Struct.*, **83**(21-22), 1780-1791.

Kianoush, M.R., Acarcan, M. and Ziari, A. (2008), "Behavior of base restrained reinforced concrete walls under volumetric change", *Eng. Struct.*, **30**(6), 1526-1534.

Kwak, H.G. and Seo, Y.L. (2002), "Time-dependent behaviour of composite beams with flexible connectors", *Comput. Method. Appl. Mech. Eng.*, **191**(34), 3751-3772.

Ma, B.G. and Gao, Y.L. (2006), "Finite element analysis for shrinkage in the interface of functionally graded concrete segment used shield tunnelling", *J. Wuhan Univ. Technol.* (Materials Science Edition), **S1**, 98-102.

Montgomery, C.J., Kulak, G.L. and Shwartsburd, G. (1983), "Deflections of a composite floor system", *Can. J. Civil Eng.*, **10**(2), 192-204.

Pałkowski, S. (2001), Konstrukcje stalowe. Wybrane zagadnienia obliczania i projektowania; Steel Structures, Some Aspects of Computation and Design; PWN, Warszawa, Poland.

Ranzi, G. (2006), "Short- and long-term analyses of composite beams with partial shear interaction stiffened by a longitudinal plate", *Steel Compos. Struct., Int. J.*, **6**(3), 237-255.

Ranzi, G. and Bradford, M.A. (2006), "Analytical solutions for the time dependent behaviour of composite beams with partial interaction", *Int. J. Solid. Struct.*, **43**(13), 3770-3793.

Ranzi, G., Leoni, G. and Zandonini, R. (2013), "State of the art on the time-dependent behaviour of

composite steel–concrete structures", *J. Construct. Steel Res.*, **80**, 252-263.
Roll, F. (1971), "Effects of differential shrinkage and creep on a composite steel–concrete structure", *ACI Special Publication*, **27**(8), 263-268.
Sakr, M.A. and Sakla, S.S.S. (2008), "Long-term deflection of cracked composite beams with nonlinear partial shear interaction: I — Finite element modelling", *J. Construct. Steel Res.*, **64**(12), 1446-1455.
Tanabe, T., Sakata, K., Mihashi, H., Sato, R., Maekawa, K. and Nakamura, H. (2009), *Creep, Shrinkage and Durability Mechanics of Concrete and Concrete Structures*, Taylor & Francis Group.
Virtuoso, F. and Vieira, R. (2004), "Time dependent behaviour of continuous composite beams with flexible connection", *J. Construct. Steel Res.*, **60**(3-5), 451-463.
Zuk, W. (1961), "Thermal and shrinkage stresses in composite beams", *Journal Proceedings*, **58**(9), 327-340.

DL